Cell, Vol. 123, 305–320, October 21, 2005, Copyright ©2005 by Elsevier Inc. DOI 10.1016/j.cell.2005.09.024

A Modular Design for the Clathrin- and Actin-Mediated Endocytosis Machinery

Marko Kaksonen,[1] Christopher P. Toret,[1] and David G. Drubin*
Department of Molecular and Cell Biology
16 Barker Hall
University of California, Berkeley
Berkeley, California 94720

Summary

Endocytosis depends on an extensive network of interacting proteins that execute a series of distinct subprocesses. Previously, we used live-cell imaging of six budding-yeast proteins to define a pathway for association of receptors, adaptors, and actin during endocytic internalization. Here, we analyzed the effects of 61 deletion mutants on the dynamics of this pathway, revealing functions for 15 proteins, and we analyzed the dynamics of 8 of these proteins. Our studies provide evidence for four protein modules that cooperate to drive coat formation, membrane invagination, actin-meshwork assembly, and vesicle scission during clathrin/actin-mediated endocytosis. We found that clathrin facilitates the initiation of endocytic-site assembly but is not needed for membrane invagination or vesicle formation. Finally, we present evidence that the actin-meshwork assembly that drives membrane invagination is nucleated proximally to the plasma membrane, opposite to the orientation observed for previously studied actin-assembly-driven motility processes.

Introduction

Endocytosis is a complex process that requires coordination of the molecular events responsible for cargo sorting, membrane invagination, vesicle scission, and vesicle targeting. A vast body of research has revealed an intricate network of numerous protein-protein interactions within the endocytic pathway, as well as many examples of functional redundancy (Engqvist-Goldstein and Drubin, 2003). Consequently, assigning specific protein functions within this pathway is challenging. Live-cell microscopy has emerged as a powerful tool to reveal protein dynamics at endocytic sites in both yeast and mammals. In mammalian cells, dynamin, actin, N-WASP, and the Arp2/3 complex have all been shown to transiently appear at clathrin-coated pits just prior to vesicle release (Merrifield et al., 2002, 2004; Yarar et al., 2005).

Many endocytic proteins in budding yeast have mammalian homologs that function in clathrin-mediated endocytosis. Several yeast endocytic proteins also colocalize with cortical actin patches, which are known to be endocytic sites (Engqvist-Goldstein and Drubin, 2003; Huckaba et al., 2004; Kaksonen et al., 2003; Sekiya-Kawasaki et al., 2003). Recently, clathrin has also been observed to transiently colocalize with cortical actin patches in yeast cells (Newpher et al., 2005).

Several yeast endocytic proteins have a dynamic spatiotemporal localization to endocytic sites (Jonsdottir and Li, 2004; Kaksonen et al., 2003; Newpher et al., 2005). The yeast homolog of WASP, Las17p, arrives earliest at the endocytic site (Kaksonen et al., 2003). While Las17p remains immotile at the cell surface, the endocytic proteins Sla1p, Pan1p (Eps15 homolog), and Sla2p (Hip1R homolog) appear at the plasma membrane after Las17p, and they move together approximately 200 nm off the cell surface (Kaksonen et al., 2003). This movement likely corresponds with coat internalization at the tip of membrane invaginations and is blocked by mutants of actin cytoskeletal proteins and by the actin inhibitor latrunculin A (LatA) (Kaksonen et al., 2003; Martin et al., 2005). Actin, Abp1p, and the Arp2/3 complex show the final type of dynamic behavior, arriving at an endocytic site as Sla1p, Pan1p, and Sla2p begin their inward movement. Actin, Abp1p, and the Arp2/3 complex persist on endocytic vesicles after Las17p, Sla1p, Pan1p, and Sla2p have disappeared, and they traverse the greatest distance before disappearing (Huckaba et al., 2004; Kaksonen et al., 2003). In addition, the type I myosin Myo5p was shown to remain immotile on the cell surface with Las17p while actin polymerizes at endocytic sites (Jonsdottir and Li, 2004).

Here we used this endocytic pathway, which was revealed by analyzing dynamics of several endocytic proteins, as a foundation and analyzed the dynamics and functions of many additional endocytic proteins to construct a detailed temporal map of endocytosis.

Results

Clathrin Localization and Function at Endocytic Sites

Similar to mammalian cells, in yeast, clathrin localizes to cortical patches that precede actin bursts (Merrifield et al., 2002; Newpher et al., 2005). However, yeast clathrin mutants show only an ~50% reduction in uptake of the endocytic cargo α factor (Chu et al., 1996; Payne et al., 1988). Therefore, a clear role for clathrin in yeast endocytosis remains to be established.

The timing of clathrin's arrival in relation to other early endocytic proteins is unclear. We colocalized GFP-tagged clathrin (Clc1-GFP) with the actin marker Abp1p tagged with monomeric red fluorescent protein (RFP) in living cells. Clc1-GFP was functional as judged by the lack of growth defects characteristic of *clc1* null mutants. Clc1-GFP localized mainly to highly dynamic internal structures but also to less motile cortical patches (Newpher et al., 2005). The cortical signal was usually masked by the strong signal from the internal structures, making imaging difficult. To overcome this problem, we used total internal reflection fluorescence (TIRF) microscopy to illuminate only the cell surface near the cover glass. Using TIRF imaging of Clc1-GFP

*Correspondence: drubin@socrates.berkeley.edu
[1]These authors contributed equally to this work.

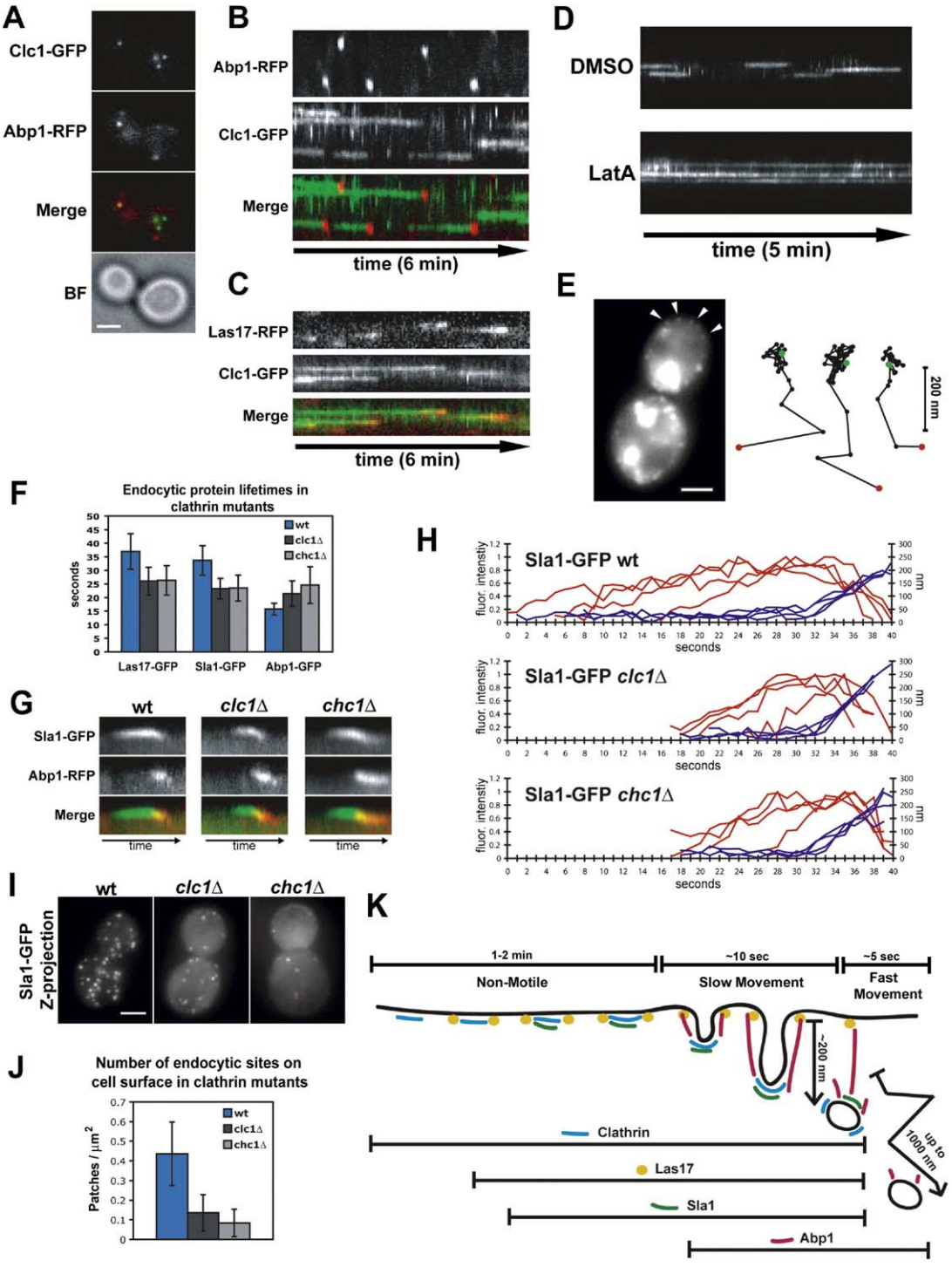

Figure 1. Clathrin Dynamics and Function at the Plasma Membrane

(A) Plasma-membrane localization of clathrin light chain (Clc1-GFP; TIRF microscopy) and Abp1-RFP (epifluorescence microscopy) in living cells. Single frame taken during simultaneous two-color imaging showing RFP fluorescence, GFP fluorescence, a merged image, and a bright-field (BF) image of the cell. Scale bar is 2 μm.

(B) Kymograph representation of two-color movie (1 frame/3 s) of cells expressing clathrin light chain (Clc1-GFP; TIRF microscopy) and Abp1-RFP (epifluorescence microscopy) in living cells, which shows cell surface patches over time as single-channel images and as a merged image. The briefly appearing (<10 s) clathrin signals are due to rapidly moving internal organelles that occasionally come into the TIRF field.

(C) Kymograph representation of two-color movie (2× binning and 1 frame/3 s) of cells expressing clathrin light chain (Clc1-GFP; TIRF microscopy) and Las17-RFP (epifluorescence microscopy) in living cells, which shows cell surface patches over time as single-channel images and as a merged image.

in combination with simultaneous epifluorescence imaging of Abp1-RFP, we were able to visualize cortical clathrin patches that partially colocalized with Abp1-RFP patches (Figures 1A and 1B; see also Movie S1 in the Supplemental Data available with this article online). The average lifetime of these cortical clathrin patches was 73.8 ± 31.5 s (n = 25 patches). Abp1-RFP joined clathrin patches, which disappeared upon Abp1-RFP arrival (Figure 1B). All clathrin patches (100%; n = 65 patches) gave rise to Abp1-RFP patches. In reverse, 98% (n = 154 patches) of Abp1-RFP patches arose from clathrin patches within the area illuminated by the evanescent wave. Clc1-GFP also preceded Las17-RFP localization to patches (Figure 1C). These data suggest that clathrin appears early at essentially all endocytic sites, preceding even Las17p. We then tested the impact of actin polymerization on clathrin dynamics using LatA. TIRF microscopy revealed that cortical Clc1-GFP patches were still present, but they were stabilized, with lifetimes typically exceeding 5 min (Figure 1D).

To determine whether clathrin patches move away from the plasma membrane, we imaged medial focal planes of the spherical yeast cells, providing views perpendicular to the plasma membrane. To circumvent challenges of imaging cortical Clc1-GFP presented by the internal structures, we used diploid cells, which are larger and therefore allowed clearer imaging of cortical clathrin structures (Figure 1E). Clc1-GFP patches moved toward the center of the cell a distance of ~200 nm before disappearing (Figure 1E). This is strikingly similar to Sla1p, Pan1p, and Sla2p patch dynamics, reinforcing the idea that this 200 nm actin-dependent movement corresponds to coat internalization.

Clathrin's endocytic role was explored by analyzing endocytic-protein dynamics in *chc1*Δ (clathrin heavy chain) and *clc1*Δ (clathrin light chain) mutants. In these mutants, Las17-GFP, Sla1-GFP, and Abp1-GFP still localized to cortical patches. However, a stronger cytoplasmic localization was observed with the early endocytic proteins Las17p and Sla1p (Figure 1I; data not shown). Also, patch lifetimes for these two proteins were reduced by 30% in the clathrin mutants (Figure 1F). In contrast, Abp1p patch lifetime was extended in clathrin mutants, often persisting slightly longer after patch movement into the cytoplasm (Figure 1F; data not shown). In clathrin mutants, Sla1-GFP patches still disappeared upon Abp1-RFP arrival (Figure 1G), and the 200 nm Sla1-GFP movement was similar to wild-type (Figure 1H). Most strikingly, clathrin mutants showed a decrease in cortical Sla1-GFP and Las17-GFP patch number (Figure 1I; data not shown). Quantification revealed 69% (*clc1*Δ) and 81% (*chc1*Δ) decreases in the number of Sla1p patches per cell surface area (Figure 1J). The shortened Sla1p patch lifetime in clathrin mutants would cause a 30% reduction in the number of patches observed at any given time. Accounting for this lifetime reduction, our results imply 56% and 73% decreases in the number of endocytic sites in *clc1*Δ and *chc1*Δ cells, respectively.

These results suggest that clathrin arrives early at all endocytic sites and aids initiating assembly of the actin-mediated internalization machinery (Figure 1K). Endocytosis still occurs in the absence of clathrin. However, the frequency at which endocytic sites are formed is reduced.

Screening Deletion Mutants

Live-cell imaging combined with powerful yeast genetics provides an attractive approach to uncover molecular mechanisms of clathrin/actin-mediated endocytosis. Given that clathrin is not required for endocytic invagination and vesicle formation in yeast, we focused on uncovering the mechanisms underlying these processes.

We used live-cell imaging to screen a set of 60 deletion mutants of endocytic genes for defects in the dynamic behavior of Sla1p (coat dynamics) and Abp1p (actin dynamics). We chose 60 nonessential proteins known either to function in endocytic internalization or to have a localization or interactions consistent with involvement in this process (Table S1). This set included *clc1*Δ and *sla2*Δ as controls (Kaksonen et al., 2003). We created strains carrying both a deletion mutation and Sla1-GFP or Abp1-GFP. Live-cell movies of each mu-

(D) Kymograph representation of TIRF-microscopy movie showing Clc1-GFP dynamics in control DMSO (top) and 200 μM LatA (bottom) treated cells.

(E) Single image of homozygous Clc1-GFP diploid cell (epifluorescence microscopy). Arrows indicate cortical Clc1-GFP patches. Scale bar, 2 μm. Tracking of three individual cortical Clc1-GFP patches. Positions of the centers of patches were determined for each frame of a movie (1 frame/s) from a medial focal plane of a cell, and consecutive positions were connected by lines. Green and red dots indicate initial and final positions, respectively. All traces are oriented so that the cell surface is up and the cell interior is down.

(F) Lifetimes of individual Las17-GFP, Sla1-GFP, and Abp1-GFP patches ± standard deviation in wild-type, *clc1*Δ, and *chc1*Δ cells. n = 30 patches for each strain. All movies were taken with 1 s frame intervals.

(G) Kymograph representations of Sla1-GFP and Abp1-RFP in a single patch from a two-color movie (1 frame/s). For wild-type, *clc1*Δ, and *chc1*Δ cells, single-channel and merged images are shown. All kymographs are oriented with cell exterior at the top.

(H) Quantification of fluorescence intensity (red) and distance from site of patch formation (blue) for Sla1-GFP patches as a function of time. Each curve represents data from one patch. Fluorescence intensity over time was corrected for photobleaching. Behavior of four independent patches was plotted for wild-type, *clc1*Δ, and *chc1*Δ strains. All movies were taken with 1 s frame intervals.

(I) Maximum intensity projections of Z stacks of wild-type, *clc1*Δ, and *chc1*Δ strains expressing Sla1-GFP. Z series was acquired though entire cell with 0.5 μm intervals. Scale bar, 2 μm.

(J) Sla1-GFP patch number/cell surface area (μm^2) ± standard deviation in wild-type, *clc1*Δ, and *chc1*Δ cells (n = 25 cells for each strain). Approximately spherical single and large budded cells with unpolarized patches were scored for each strain. Surface area of individual cells was estimated as an average of sphere surface areas calculated from four diameters (at 0°, 45°, 90°, and 135°) measured from maximum intensity projections.

(K) Model depicting pathway of clathrin/actin-mediated endocytosis in yeast.

Green (GFP) and red (RFP) in all merges of two-color images and kymographs.

tant were visually analyzed for changes in localization or temporal behavior of the marker proteins. Clear abnormalities in the dynamic behavior of either or both of the marker proteins were seen in 14 of the 60 mutants (Table S1; Figure S1; Movies S2 and S3). While defects in endocytic uptake have been reported for ten of these mutants, no such defects have been observed for *cap1*Δ, *cap2*Δ, *bbc1*Δ, and *abp1*Δ (Table S1). Thus, our in vivo dynamics analyses are more sensitive than analyses used in previous studies. Distinct Sla1-GFP or Abp1-GFP phenotypes were observed in different mutants, suggesting that the endocytic proteins function at different steps along the endocytic pathway (Table S1).

Coat-Complex and Actin-Patch Dynamics in Endocytic Deletion Mutants

We chose nine mutants (*sla1*Δ, *end3*Δ, *bbc1*Δ, *rvs161*Δ, *rvs167*Δ, *sac6*Δ, *cap1*Δ, *cap2*Δ, and *abp1*Δ) for more in-depth analysis because they showed defects that suggested functions during the actin-driven invagination and vesicle-formation processes. Three other mutants (*sla2*Δ, *arc18*Δ, and *vrp1*Δ) had phenotypes indicating roles in these processes. The phenotypes of *sla2*Δ and Arp2/3 complex mutants have been described previously (Kaksonen et al., 2003; Martin et al., 2005), and in-depth analysis of *vrp1*Δ will be reported separately (Y. Sun, A.C. Martin, and D.G.D., unpublished data). Similar to clathrin mutants, *ede1*Δ mutants had reduced Sla1p patch lifetimes and fewer endocytic sites, which suggests that Ede1p functions prior to coat internalization (Figures S1 and S2).

The nine gene deletions were analyzed in strains expressing Sla1-GFP and/or Abp1-RFP. For the *sla1*Δ and *abp1*Δ strains, we used Pan1-GFP and Sac6-RFP, respectively, as surrogate markers (Doyle and Botstein, 1996; Kaksonen et al., 2003). To begin, we measured the mean lifetime of both Sla1/Pan1-GFP and Abp1/Sac6-RFP patches in mutants expressing one fluorescent marker protein. All mutants showed increased patch lifetimes compared to wild-type cells ($p < 0.001$, except Abp1-RFP in *bbc1*Δ $p < 0.05$; Figure 2A). However, the patch lifetimes were differentially affected by different mutations. We then analyzed the dynamic behavior of these proteins in live cells (Figure 2B; Movie S4).

The endocytic adaptor protein Sla1p and the EH domain protein End3p form a complex with Pan1p (Tang et al., 2000). Sla1p can also inhibit Arp2/3 activation by Las17p in vitro (Rodal et al., 2003). Deletions of either protein caused similar phenotypes. Consistent with earlier findings (Warren et al., 2002), in *end3*Δ cells, Sla1-GFP was mostly cytoplasmic and localized poorly to cortical patches (Figure S1; Movie S2). Due to weak Sla1-GFP localization in this strain, we used Pan1-GFP as a marker. Pan1-GFP also localized weakly to cortical patches as seen before (Tang et al., 1997), but it was not as severely affected as Sla1-GFP. In *sla1*Δ and *end3*Δ mutants, Pan1-GFP moved off the cell surface when Abp1p arrived, and the rate and distance of movement were normal. However, Pan1-GFP patch lifetimes were greatly increased and more variable than in wild-type cells (Figure 2A). As described earlier, both mutants also contained fewer and larger Abp1-RFP patches compared to wild-type cells (Holtzman et al., 1993). These data suggest that Sla1p and End3p might regulate the initiation of actin polymerization at endocytic sites.

The SH3 domain protein, Bbc1p (also known as Mti1p), interacts with the type I myosins, Myo3p and Myo5p; colocalizes with actin patches (Mochida et al., 2002); and inhibits Las17p in vitro (Rodal et al., 2003). Deletion of *BBC1* caused the speed and the distance of the inward Sla1p movement to increase (Figure 2B). Onset of this movement correlated with arrival of Abp1-RFP, which also moved at a similar speed (Figure 2B; data not shown). These data suggest that Bbc1p regulates coat-complex internalization at endocytic sites, possibly by regulating actin nucleation via Las17p or Myo3/5p.

Rvs161p and Rvs167p are yeast amphiphysins (Sivadon et al., 1995). Mammalian amphiphysin can tubulate membranes, and it is thought to link dynamin to the clathrin coat (Takei et al., 1999). Both *rvs161*Δ and *rvs167*Δ cells had similar phenotypes (Figure 2B and Figure S1; Movies S2 and S3). The majority of the Sla1-GFP patches in these mutants were internalized normally. However, 28.3% (n = 145 patches) of the Sla1-GFP patches in *rvs167*Δ cells and 33.1% (n = 145) in *rvs161*Δ cells began to move off the cell surface but then retracted toward the cell surface (Figure 2B and Figure S1). A similar number of Sla1-GFP retractions were observed in the *rvs161*Δ *rvs167*Δ double null (24.8%, n = 109), suggesting that both proteins are required for functionality. The retraction took place after the Sla1-GFP patch had internalized and when the patch intensity had already decreased significantly from the peak intensity. Thus, it is likely that we failed to see a portion of these retraction movements and underestimated their frequency. Retraction movements were very rarely seen in wild-type cells (0.7%, n = 136 patches). Interestingly, Abp1-RFP fluorescence intensity peaks when the Sla1-GFP patch retracts, yet Abp1-RFP patches did not show similar retractions (Figure 2B). Given the reported activities of amphiphysin, the abortive internalization observed in these mutants may be due to a failure in scission after actin-driven invagination, after which membrane tension retracts the endocytic coat, but not the actin meshwork, back to the cell cortex.

Sac6p is yeast fimbrin, an actin-filament-crosslinking protein (Adams et al., 1991). In *sac6*Δ cells, Sla1-GFP's inward movement was completely abolished even though the actin marker Abp1-RFP was still recruited to Sla1-GFP sites in a manner similar to in wild-type cells (Figure 2B). Correspondingly, the fast Abp1p patch movement was lost (Movie S4). These data suggest that actin-filament crosslinking is essential for productive force generation at endocytic sites.

Cap1p and Cap2p are the α and β subunits of yeast actin-capping protein and are both required for capping function (Amatruda et al., 1992). In agreement with this, *cap1*Δ and *cap2*Δ cells showed similar phenotypes. Sla1-GFP patches moved in at reduced speed (Figure 2B). Additionally, Abp1-RFP patches were brighter, as described previously (Kim et al., 2004). Notably, these mutants showed the longest Abp1-RFP lifetimes of any mutants analyzed in this study (Figure 2A). Capping

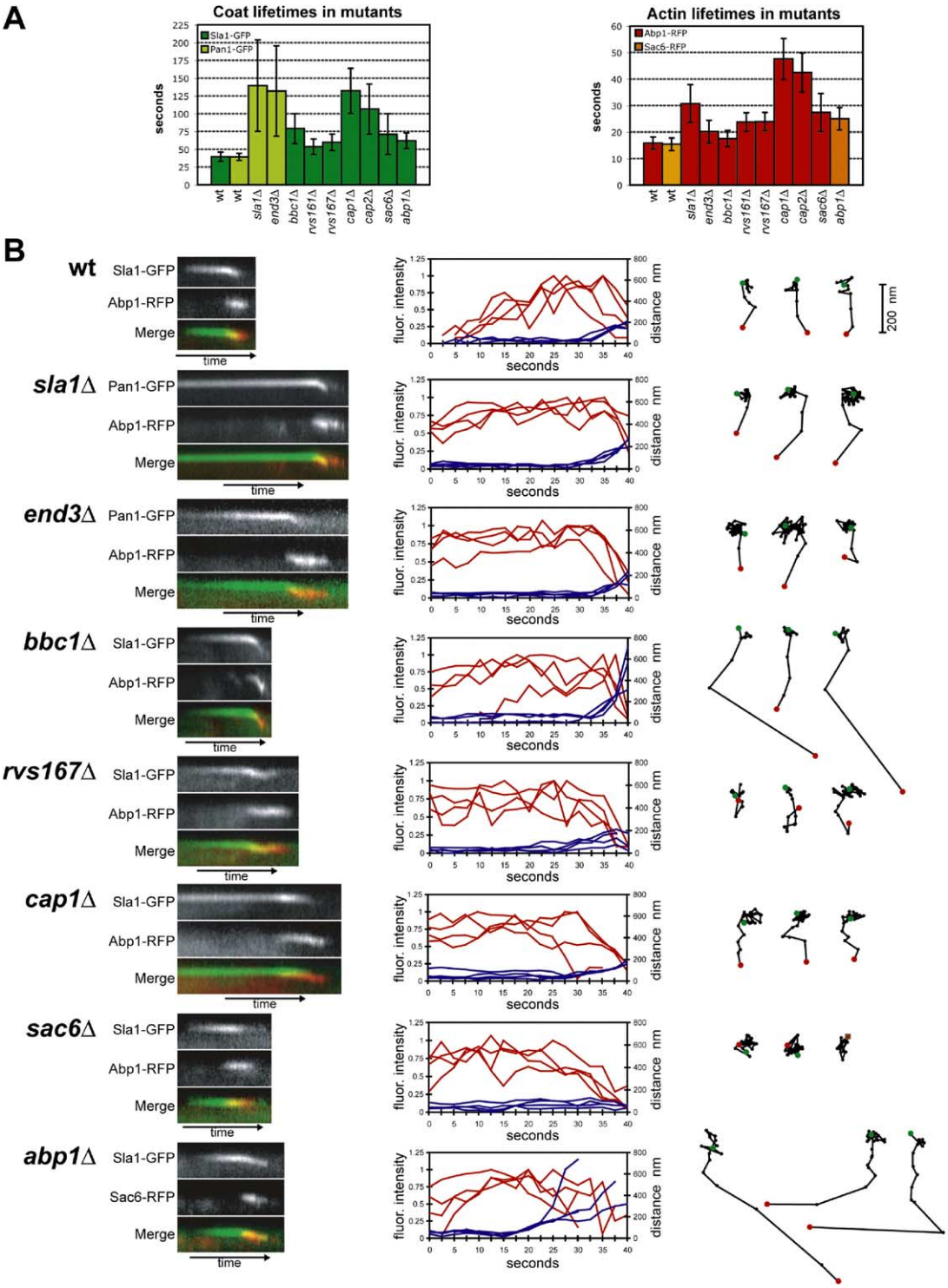

Figure 2. Sla1-GFP and Abp1-RFP Dynamics in Endocytic Mutant Cells

(A) Lifetimes of individual Sla1-GFP or Pan1-GFP patches (left) and Abp1-RFP or Sac6-RFP patches (right) ± standard deviation in wild-type and mutant cells. n = 32 patches for each strain. Sla1-GFP/Pan1-GFP movies were taken with 2.5 s frame intervals, and Abp1-RFP/Sac6-RFP movies were taken with 1 s frame intervals.

(B) Analysis of coat and actin dynamics in wild-type and endocytic mutant cells. Left column shows kymograph representations of Sla1-GFP or Pan1-GFP and Abp1-RFP or Sac6-RFP of a single patch from a two-color movie (1 frame/s). For each strain, single-channel and merged images (GFP = green and RFP = red) are shown. All kymographs are oriented with cell exterior at the top. Center column shows quantification of fluorescence intensity (red) and distance from site of patch formation (blue) for Sla1-GFP patches as a function of time. Each graph shows the last 40 s of each patch lifetime. Each curve represents data from one patch. Fluorescence intensity over time was corrected for photobleaching. Behavior of four independent patches was plotted for each strain. Right column shows tracking of three Sla1-GFP patches for each strain. Positions of the centers of patches were determined for each frame of a movie (1 frame/2.5 s) from a medial focal plane of a cell, and consecutive positions were connected by lines. Green and red dots indicate initial and final positions, respectively, for each Sla1p patch. All traces are oriented so that the cell surface is up and the cell interior is down.

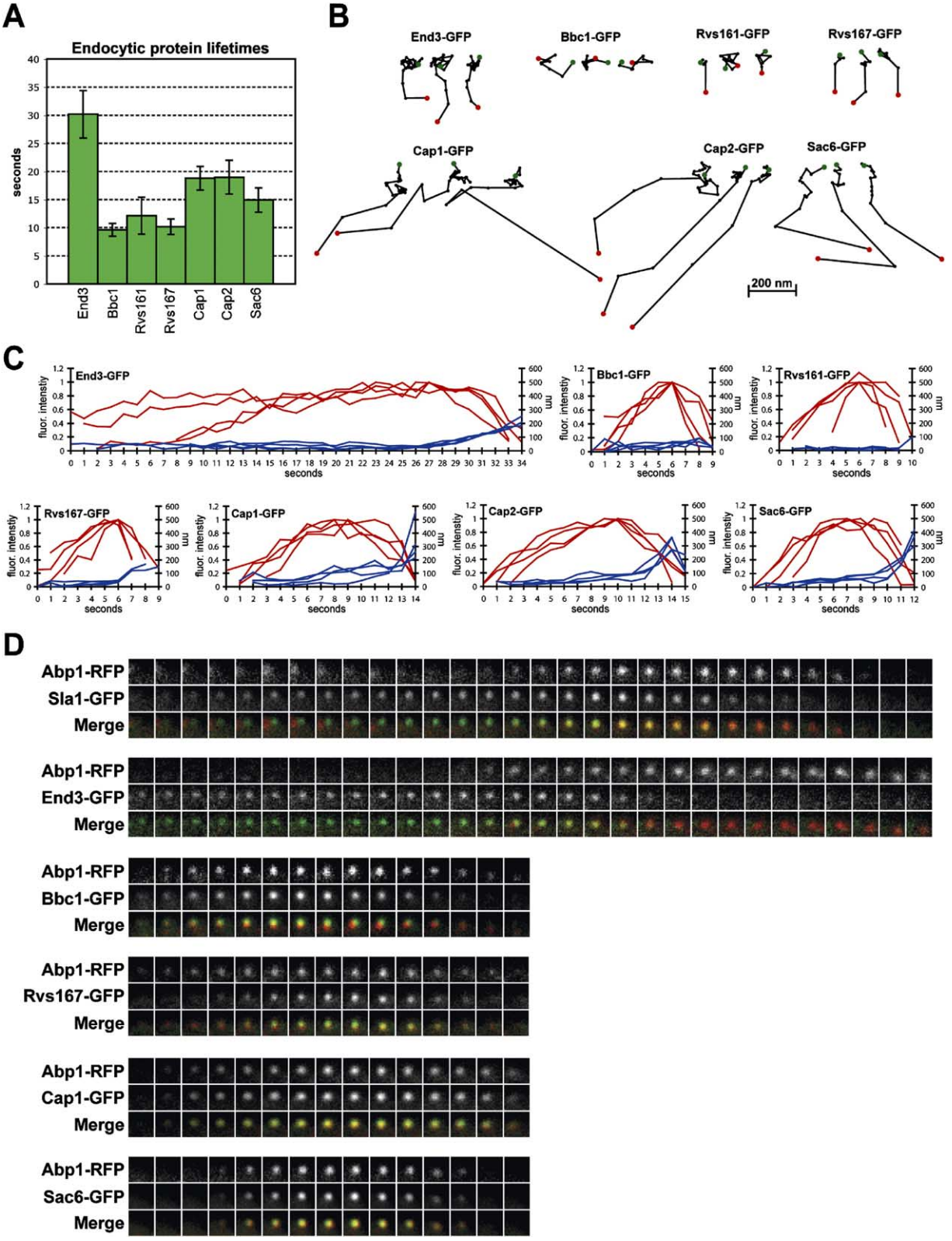

Figure 3. Protein Dynamics at Endocytic Sites

(A) Lifetimes for different GFP-tagged endocytic proteins ± standard deviation. n = 35 patches for each protein. All movies were taken with 1 s frame intervals.

(B) Particle tracking for endocytic proteins. Positions of the centers of patches were determined for each frame of a movie (1 frame/s) from

protein may facilitate actin-driven coat-complex movement by funneling monomeric actin to the barbed ends of newly nucleated filaments (Pantaloni et al., 2001).

Abp1p is an F-actin binding protein that can activate the Arp2/3 complex (Goode et al., 2001). In *abp1*Δ cells, the initial slow movement of Sla1-GFP was normal (Figure 2B). In wild-type cells, Sla1p dissipated from patches during the slow inward movement. However, in *abp1*Δ cells, Sla1-GFP persisted after the slow movement and then showed a fast movement characteristic of actin patches in wild-type cells (Figure 2B). In *abp1*Δ cells, Sac6-RFP also persisted longer in the cytoplasm, colocalizing with the rapidly moving Sla1-GFP patches (Movie S4). The Sac6-RFP patches occasionally fused with neighboring patches. These data suggest that Abp1p likely functions to disassemble endocytic structures.

We next analyzed effects of the nine deletion mutations on clathrin-patch dynamics. TIRF imaging of clathrin together with epifluorescence imaging of Abp1-RFP revealed that clathrin-patch lifetimes were dramatically extended in *sla1*Δ, *end3*Δ, and *sac6*Δ cells. In *sla1*Δ and *end3*Δ cells, the long-lived clathrin patches, similar to Pan1-GFP, consistently terminated with Abp1-RFP bursts (Figure S3A). In *sac6*Δ cells, Abp1-RFP bursts took place at clathrin patches. However, unlike Sla1p, the clathrin patches often remained stable after the Abp1-RFP burst, suggesting that the failure to invaginate the plasma membrane may lead to a defect in clathrin disassembly (Figure S3A). The other mutants did not dramatically alter clathrin dynamics (Figure S3A). These data are consistent with observations that clathrin accumulates at the cell cortex in *end3*Δ but not in *rvs161*Δ or *rvs167*Δ (Newpher et al., 2005). We also imaged clathrin using epifluorescence microscopy. Clc1-GFP showed qualitatively similar behavior to Sla1-GFP in *rvs161*Δ, *rvs167*Δ, and *bbc1*Δ strains (Figure S3B). Detailed analysis of Clc1-GFP movement in *cap1*Δ, *cap2*Δ, *sac6*Δ, and *abp1*Δ cells was hindered by the strong signal from the internal clathrin structures.

Dynamic Localization of Endocytic Proteins

Given the unique deletion phenotypes of these nine proteins, we next quantitatively analyzed the spatial and temporal localization of C-terminal GFP fusions of each protein expressed from its endogenous locus. None of the GFP fusions showed any of the phenotypes seen in the corresponding deletion mutants (e.g., slower growth or changes in Abp1p dynamics; data not shown), demonstrating that the fusion proteins are functional. We analyzed the behavior of each fusion protein individually, and then together with Abp1-RFP, to determine the temporal order of protein recruitment to endocytic sites (Figure 3; Movie S5). The dynamic behaviors fell into four distinct groups described below.

In the first group, End3-GFP had a lifetime of 30.2 ± 4.2 s (Figure 3A). It initially formed an immotile patch that later moved about 200 nm toward the cell center while it was dissipating (Figures 3B and 3C). The onset of the inward movement corresponded with the arrival of Abp1-RFP at the End3-GFP patch (Figure 3D). Thus, End3p behaves like Sla1p, Pan1p, and Sla2p (Kaksonen et al., 2003). Since these proteins move like clathrin, they are likely associated with the vesicle coat.

In the second group, Bbc1-GFP patches had a short lifetime of 9.6 ± 1.1 s and stayed immotile at the cell surface throughout their lifetime (Figures 3A–3C). This behavior is similar to what has been described for Myo5p (Jonsdottir and Li, 2004) and Las17p, although Las17p patches have a longer lifetime of ~40 s (Kaksonen et al., 2003). Simultaneous, two-color analysis with Abp1-RFP revealed that Bbc1-GFP arrives when actin begins to polymerize (Figure 3D), similar to Myo5-GFP (Jonsdottir and Li, 2004).

In the third group, Rvs161-GFP and Rvs167-GFP also appeared at patches very transiently (12.1 ± 3.3 and 10.2 ± 1.4 s respectively; Figure 3A). These proteins were initially immotile, then moved and immediately dissipated from the patch (Figures 3B and 3C). The patch centroids moved only about 100 nm, and the movement took place in less than 0.5 s (Figures 3B and 3C; data not shown). Rvs161-GFP also showed strong diffuse cytoplasmic staining, which reduced the contrast of patches, making it difficult to determine if all Rvs161-GFP patches moved. Simultaneous two-color analysis revealed that the Rvs proteins arrive at the patch after Abp1-RFP (Figure 3D).

In the fourth group, Cap1-GFP, Cap2-GFP, and Sac6-GFP formed patches with lifetimes of 18.8 ± 2.1, 19.0 ± 3.0, and 14.9 ± 2.2 s, respectively (Figure 3A). They colocalized well with Abp1-RFP and showed similar dynamics of recruitment and disassembly and similar motility behaviors (Figures 3B–3D). However, the capping-protein lifetimes suggest that they may persist slightly longer than Abp1p and Sac6p.

F-Actin Dependence for Endocytic-Protein Localization

Some endocytic proteins are known to depend on F-actin for their localization or turnover at cortical patches. To test if the F-actin dependency correlates with the groupings revealed by analysis of protein behaviors (Figure 3), we used LatA treatment to disrupt the actin cytoskeleton and analyzed behavior of the GFP fusion proteins in living cells. To monitor the efficiency of the LatA treatment, we coexpressed Abp1-RFP, which requires F-actin for its localization (Ayscough et al., 1997).

a medial focal plane of a cell, and consecutive positions were connected by lines. Green and red dots indicate initial and final positions, respectively, for each patch. All traces are oriented so that the cell surface is up and the cell interior is down.

(C) Quantification of fluorescence intensity (red) and distance from site of patch formation (blue) as a function of time for patches of each GFP-tagged endocytic protein. Each curve represents data from one patch. Fluorescence intensity over time was corrected for photobleaching. Behavior of four independent patches was plotted for each strain. All movies were taken with 1 s frame intervals.

(D) Dynamic localization of GFP-tagged proteins in reference to Abp1-RFP in living cells. Time series showing composition of individual patches from two-color movies (1 frame/s). Upper and middle rows show two separate channels, and lower panel shows merged images.

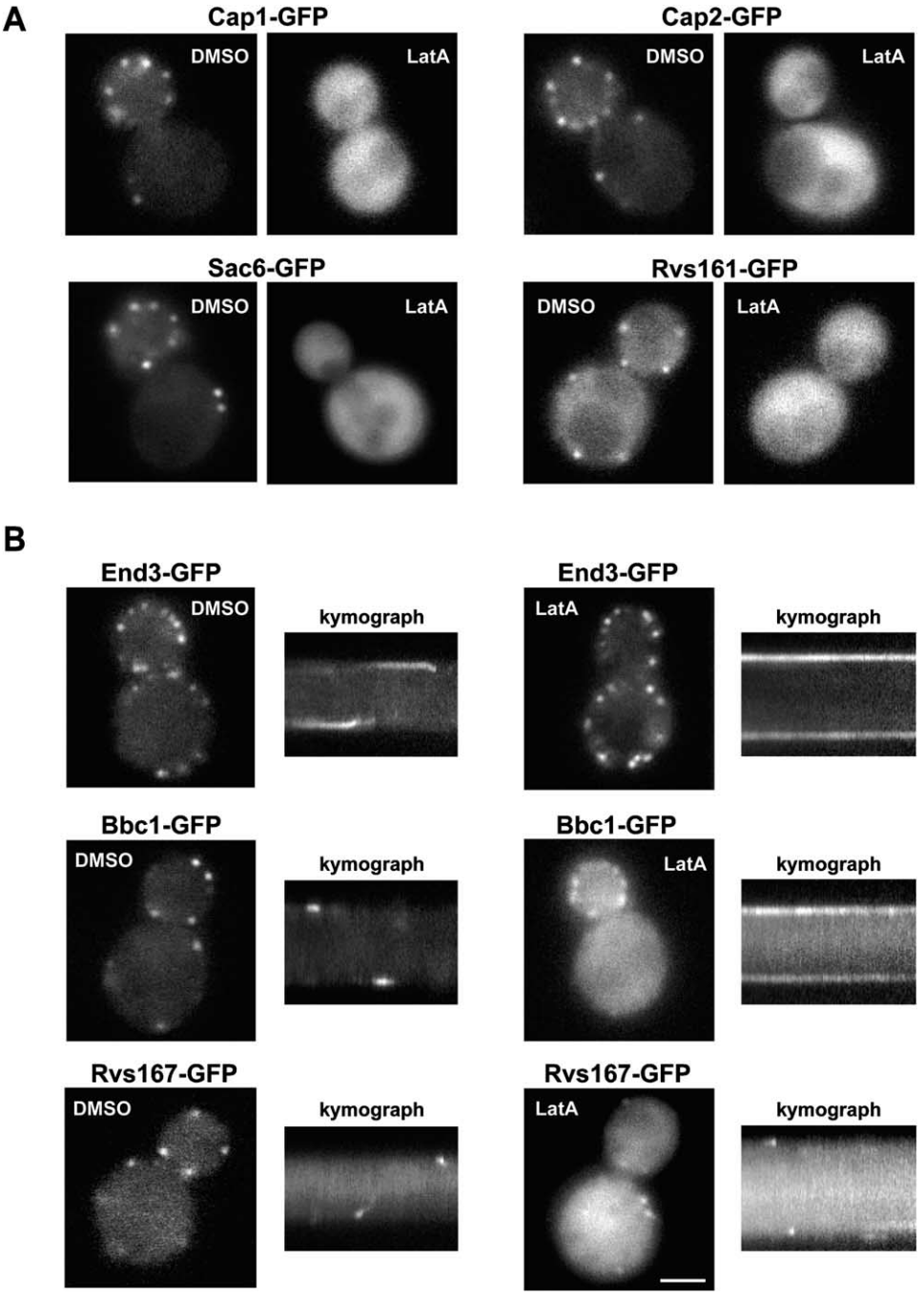

Figure 4. Endocytic Protein Localization and Dynamics in the Absence of F-Actin

(A) Localization of GFP-tagged endocytic proteins in the presence of 200 μM LatA or DMSO.
(B) Single frames from live-cell movies showing localization of GFP-tagged endocytic proteins in the presence of 200 μM LatA or DMSO with corresponding kymographs on right. Each kymograph shows dynamics of two patches on opposite sides of a cell for 2 min. Scale bar, 2 μm.

Cap1-GFP, Cap2-GFP, Sac6-GFP, and Rvs161-GFP became completely diffuse in LatA-treated cells (Figure 4A), showing that actin filaments are needed for their localization. In contrast, Bbc1-GFP, End3-GFP, and Rvs167-GFP still appeared in cortical patches in LatA (Balguerie et al., 1999). However, both Bbc1-GFP and Rvs167-GFP showed increased cytoplasmic localization, suggesting that they may depend partially on actin for their localization. We then studied how LatA affects dynamics of these proteins. Bbc1-GFP and End3-GFP were highly stable and immotile, suggesting that they are capable of localizing independently of F-actin but require actin for disassembly from patches (Figure 4B). In contrast to Rvs161-GFP, Rvs167-GFP formed patches

in LatA, and the patches assembled and disassembled very rapidly (average lifetime of 7.6 ± 4.7 s; n = 25; Figure 4B), a behavior so far unique among endocytic proteins.

Regulation of Actin Polymerization by Sla1p and Bbc1p

Bbc1p and Sla1p inhibit Las17p's Arp2/3-activating activity in vitro (Rodal et al., 2003). Each mutant phenotype was also consistent with defects in the regulation of actin nucleation (Figure 2B), suggesting that these two proteins may cooperate in the regulation of actin polymerization. When we combined *bbc1*Δ and *sla1*Δ mutations, long Abp1-RFP-labeled actin protrusions extended dynamically from the cell surface (Figure 5A; Movie S6). A *bbc1*Δ *end3*Δ double mutant showed similar actin structures (data not shown), consistent with our earlier observations that *end3*Δ and *sla1*Δ have similar phenotypes and that Sla1p is poorly localized in *end3*Δ cells.

To visualize the coat in relation to these unusual actin protrusions, we coexpressed either Pan1-GFP or Clc1-GFP with Abp1-RFP in *bbc1*Δ *sla1*Δ cells. Initially, Abp1-RFP-labeled actin clouds formed around Pan1/Clc1-GFP patches. Then, continuing actin assembly formed protrusions that pushed the actin-cloud-covered Pan1/Clc1-GFP patches into the cytoplasm (Figures 5A–5C; Movie S6). The Pan1/Clc1-GFP patches and their surrounding actin clouds disassembled first, leaving only the dynamic actin protrusions, which persisted slightly longer before disassembling. The movements of Pan1p and Clc1p patches in *bbc1*Δ *sla1*Δ cells are qualitatively similar to their actin-dependent movements in wild-type cells. However, the actin structures were greatly exaggerated, often spanning half of a cell diameter (Figure 5A). To address whether these coat-complex proteins associate with endocytic vesicles, we visualized the vital membrane dye, FM4-64, in *bbc1*Δ *sla1*Δ cells expressing Pan1-GFP. FM4-64 labels endocytic vesicles and colocalizes with internalizing Abp1p in wild-type cells (Huckaba et al., 2004). As expected, in these mutants, Pan1-GFP patches colocalized with FM4-64-labeled vesicles (Figure 5D). Additionally, the FM4-64-labeled vesicles persisted after Pan1-GFP had disassembled (Figure 5D).

The large size of these abnormal actin protrusions allowed us to use photobleaching to study the directionality and rate of actin polymerization. We expressed actin-GFP from a plasmid in *bbc1*Δ *sla1*Δ cells and photobleached small regions of the actin protrusions. The bleached regions moved away from the membrane toward the cell center at 92 ± 20 nm/s (n = 16) (Figure 5E; Movie S7), demonstrating that actin monomers are added at the plasma membrane and that growing filaments then push the endocytic coat complex off the plasma membrane.

As Bbc1p and Sla1p can potentially regulate Las17p activity, we localized Las17-GFP in the mutants. Surprisingly, in *bbc1*Δ mutants, Las17-GFP patches occasionally split, so that the majority remained at the plasma membrane while a portion moved into the cell (Figure 5F). In *sla1*Δ mutant cells, both Las17p and Abp1p formed patches that were somewhat brighter than in wild-type cells but that behaved relatively normally (Figure 5F). In *bbc1*Δ *sla1*Δ double mutants, Las17-GFP patches became much brighter when actin started polymerizing. Also, part of the Las17-GFP patch often moved into the cell at the tip of the actin protrusion (Figure 5F; Movie S6). The increased accumulation of Las17-GFP is consistent with its being involved in formation of the actin protrusions. We suspect that in wild-type cells a similar actin-based mechanism drives endocytic invagination.

Invagination/Scission Relationship

We next wanted to study in more detail the putative scission process involving Rvs161p and Rvs167p. Absence of either protein leads to frequent retraction of internalized coat complexes back to the plasma membrane, possibly due to failed scission (Figure 2B and Figures S1 and S3).

The enhanced coat movement seen in *bbc1*Δ cells may happen before or after scission. To address this issue, we analyzed the movement of Sla1-GFP in *rvs167*Δ *bbc1*Δ double-mutant cells. Interestingly, in the double mutant, all patches that retracted behaved in a manner similar to patches in the *rvs167*Δ single mutant, retracting after moving ~200 nm (Figure 6A; Movie S8). This suggests that the enhanced actin-driven movement in *bbc1*Δ mutants happens mostly after the Rvs proteins function.

Rvs161-GFP and Rvs167-GFP reach their maximum fluorescence intensity at the same time as Abp1-RFP at endocytic sites (Figure 6B; data not shown). Rvs167-GFP patches move immediately after their intensity peaks, and this movement is shorter and faster than coat movements (Figures 3 and 6C). This movement could correspond to vesicle scission. The timing is consistent with recent observations in mammalian cells in which scission occurs concomitant with peak actin recruitment at endocytic sites (Merrifield et al., 2005). We tested whether this movement is dependent on actin polymerization. Although LatA did not block the transient localization of Rvs167-GFP (Figure 4B), it resulted in inhibition of Rvs167-GFP patch movement (Figure 6D). In *sac6*Δ cells, in which coat internalization is blocked (Figure 2B), Rvs167-GFP patches were also immotile, although they still formed and disappeared rapidly (Figure 6D). Interestingly, Rvs161-GFP showed behavior similar to Rvs167-GFP in *sac6*Δ cells (data not shown), which was in contrast with its behavior in LatA-treated cells. We also studied the behavior of Rvs167-GFP in *bbc1*Δ cells. In these cells, Rvs167-GFP patches moved much further into the cell, suggesting that altered actin dynamics also affects Rvs167-GFP disassembly (Figure 6D).

To further analyze the behavior of the Rvs proteins, we expressed Rvs167-GFP and Abp1-RFP in *bbc1*Δ *sla1*Δ cells, which exhibit enlarged actin patches (Figure 5). As in wild-type cells, Rvs167-GFP localized to endocytic sites slightly after Abp1-RFP. Interestingly, Rvs167-GFP patches often elongated into tubular structures within the actin plumes. After elongating, the tip of these Rvs167-GFP structures frequently separated and moved inward with the growing actin protrusion. The remaining cortically associated part of the Rvs167-

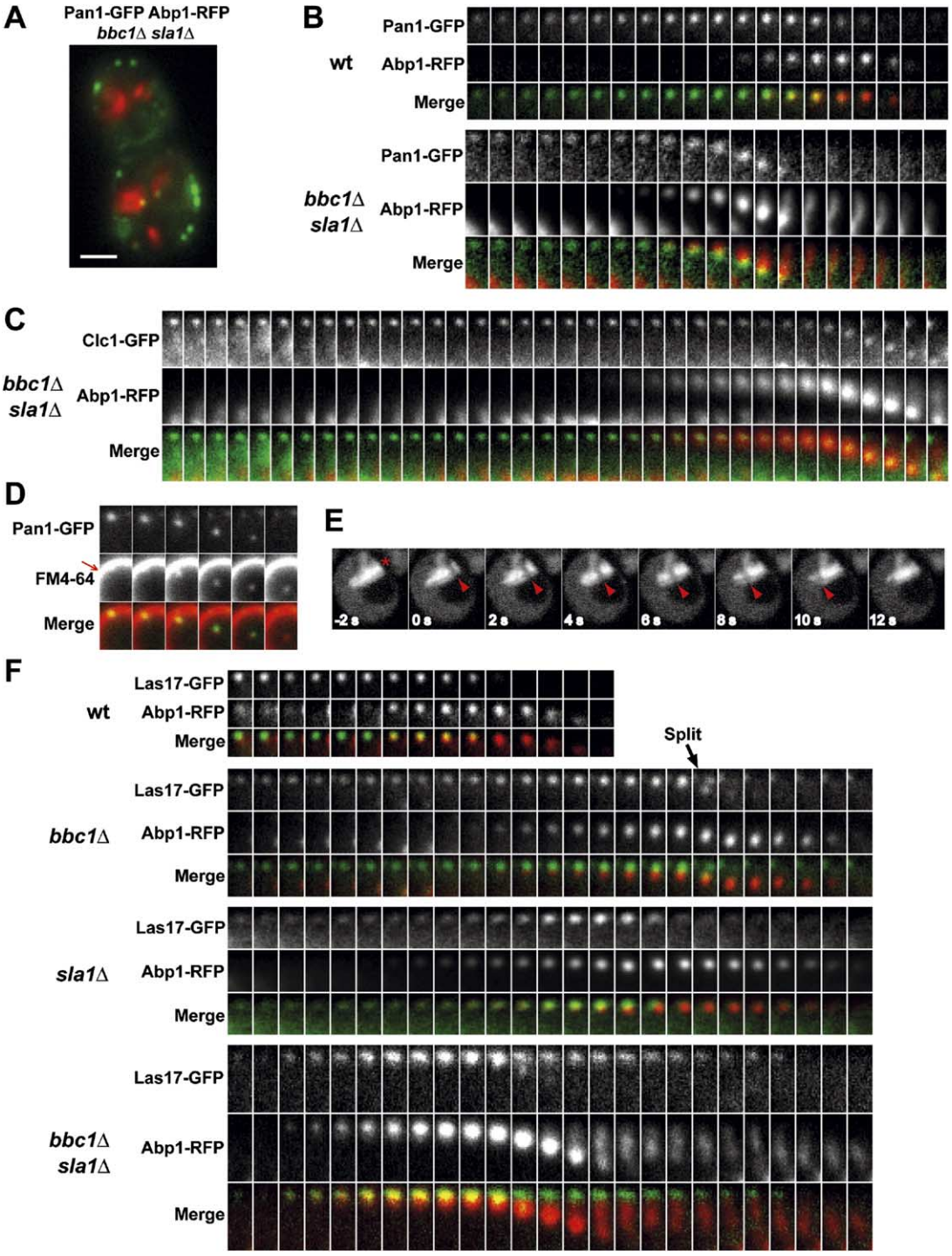

Figure 5. Actin-Driven Endocytic Internalization in Cells Lacking Las17p Regulators

(A) Single frame from two-color movie showing Pan1-GFP (green) and Abp1-RFP (red) in *bbc1*Δ *sla1*Δ cells. Scale bar, 2 μm.

(B) Time series showing individual Pan1-GFP/Abp1-RFP patches in wild-type (top) and *bbc1*Δ *sla1*Δ (bottom) cells from two-color movies (1 frame/2 s). Each time series shows Pan1-GFP in the top panel, Abp1-RFP in the middle panel, and a merged image in the bottom panel.

(C) Time series showing individual Clc1-GFP/Abp1-RFP patches in *bbc1*Δ *sla1*Δ cell from two-color movie (1 frame/2 s). Time series shows Clc1-GFP in the top panel, Abp1-RFP in the middle panel, and a merged image in the bottom panel.

(D) Time series showing a Pan1-GFP patch in a cell stained with FM4-64 (1 frame/6 s). Time series shows Pan1-GFP in the top panel, FM4-64 staining in the middle panel, and merged image in the bottom panel. Red arrow indicates the plasma membrane.

(E) Time series showing 2 s intervals of FRAP in *bbc1*Δ *sla1*Δ cells expressing Act1-GFP. Photobleached bar is indicated by red arrowhead and the site of connetion between actin protrusion and cell surface by asterisk.

(F) Time series showing individual Las17-GFP/Abp1-RFP patches in wild-type, *bbc1*Δ, *sla1*Δ, and *bbc1*Δ *sla1*Δ cells from two-color movies (1 frame/2 s). Each time series shows Las17-GFP in the top panel, Abp1-RFP in the middle panel, and a merged image in the bottom panel. Arrow indicates Las17-GFP splitting in *bbc1*Δ cells.

Time series in (B), (C), and (F) are oriented with cell exterior at the top. GFP is show in green and RFP or FM4-64 in red in all two-color merges.

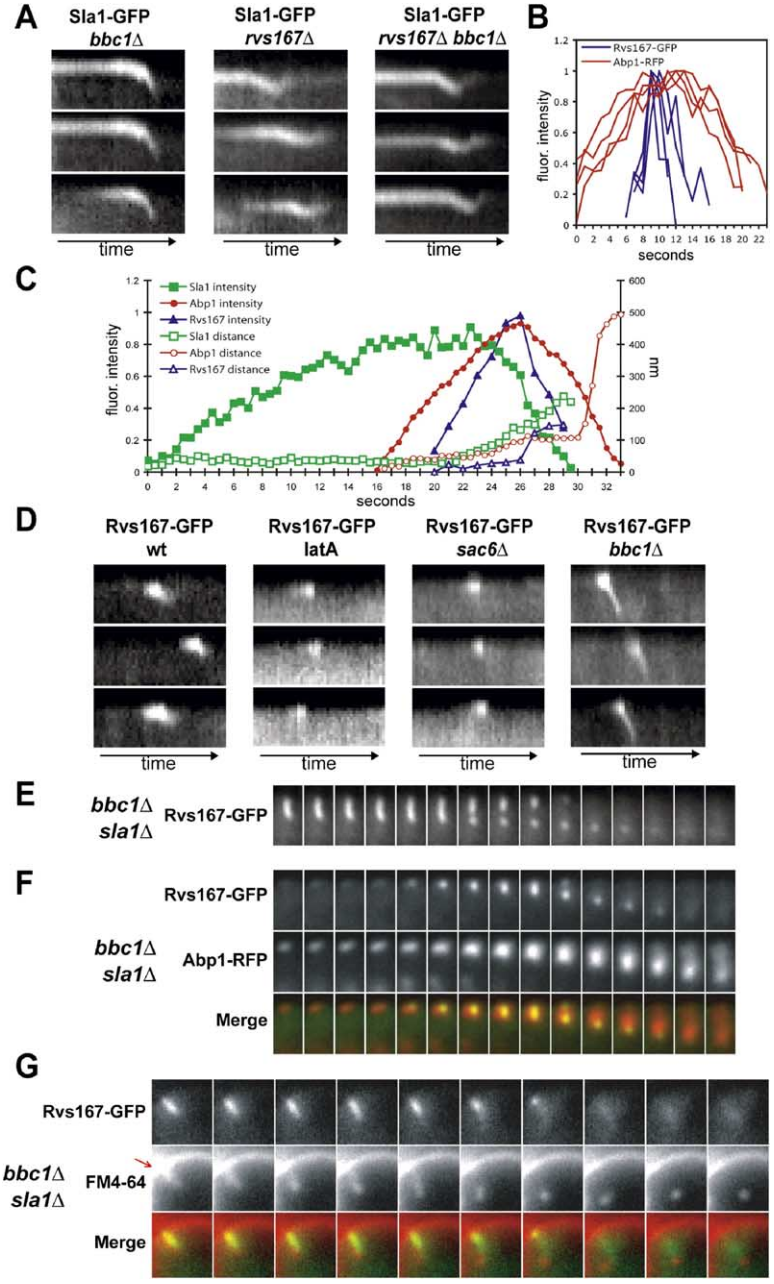

Figure 6. Scission Dynamics in Endocytic Mutants

(A) Kymograph representation of Sla1-GFP in live-cell movies (1 frame/s) in *bbc1*Δ (left), *rvs167*Δ (center), and *rvs167*Δ *bbc1*Δ double-mutant (right) cells. Each panel shows three individual patches.

(B) Change of relative fluorescence intensities over time from four independent patches in cells expressing Rvs167-GFP and Abp1-RFP. Intensities are from two-color movies (1 frame/s).

(C) Average fluorescence intensity and average distance from site of patch formation as a function of time for Rvs167p, Sla1p, and Abp1p patches. S1a1p and Abp1p data are from Kaksonen et al. (2003). Rvs167p data were determined from four individual patches in cells expressing Rvs167-GFP (1 frame/s) and aligned to the Abp1p peak intensity in the plot.

(D) Kymograph representation of Rvs167-GFP in live-cell movies (1 frame/s) in wild-type (left), LatA-treated (left center), *sac6*Δ mutant (right center), and *bbc1*Δ mutant (right) cells. Each panel shows three individual patches.

(E) Time series showing Rvs167-GFP tubule in *bbc1*Δ *sla1*Δ cell (1 frame/s).

(F) Time series showing Rvs167-GFP and Abp1-RFP in *bbc1*Δ *sla1*Δ cell (1 frame/s).

(G) Time series showing Rvs167-GFP in FM4-64-stained *bbc1*Δ *sla1*Δ cell (1 frame/1.5 s). Red arrow indicates the plasma membrane.

Kymographs and time series in (A) and (D)–(F) are oriented with cell exterior at the top. GFP is shown in green and RFP or FM4-64 in red in all two-color merges.

GFP tubule receded toward the plasma membrane and disappeared (Figures 6E and 6F). FM4-64 staining of *bbc1*Δ *sla1*Δ mutants revealed that Rvs167-GFP colocalized with membrane tubules that emanated from the plasma membrane and produced vesicles (Figure 6G).

Discussion

Clathrin in Yeast Endocytosis

A direct clathrin function in yeast endocytosis had not previously been established (Baggett and Wendland, 2001). Our results demonstrate that clathrin is an integral component of the yeast actin-dependent endocytic pathway. Advancing on recent observations (Newpher et al., 2005), we found that clathrin precedes all previously described yeast endocytic proteins to endocytic sites and that virtually all endocytic sites contain both clathrin and actin (Figure 1). Thus, it is unlikely that there is an alternative, clathrin-independent, actin-dependent endocytic pathway in wild-type yeast cells. Moreover, we observed that clathrin patches internalize about 200 nm before disappearing. We presume that the 200 nm clathrin movement corresponds to clathrin-coated-pit and clathrin-coated-vesicle formation (Figure 7). In mammalian cells, a portion of clathrin-coated pits disassemble without undergoing internalization (Ehrlich et al., 2004). However, we did not detect abortive clathrin patches in budding yeast.

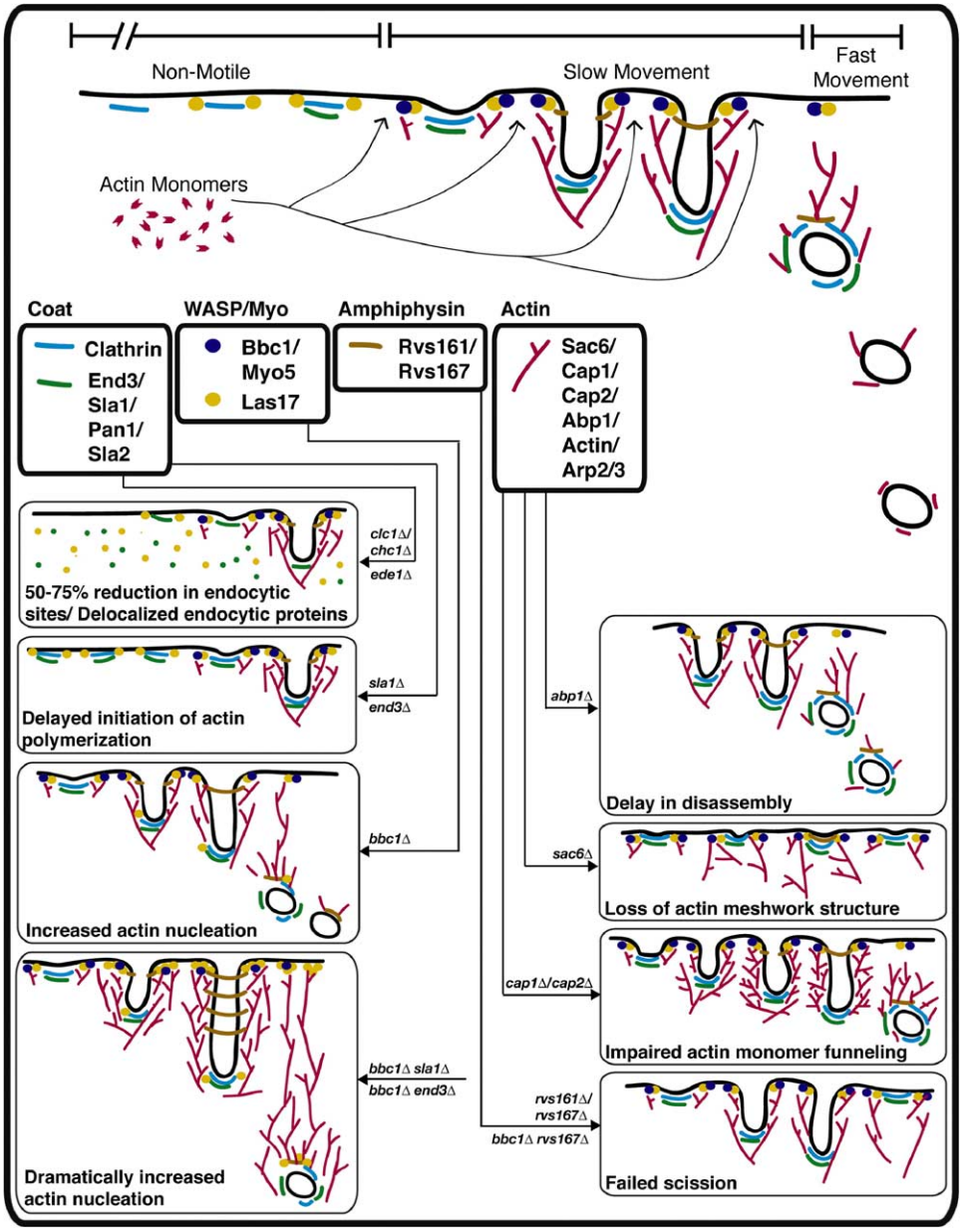

Figure 7. Modular Design of Clathrin/Actin-Mediated Endocytosis in Yeast
See text for description.

Although not required for invagination and vesicle formation in yeast, clathrin plays a crucial role in efficient initiation of endocytic-site assembly (Figure 1). The reduced rate of receptor-mediated endocytosis in clathrin mutants (Chu et al., 1996; Payne et al., 1988) can be explained by the ~50%–75% reduction in the number of endocytic sites (Figures 1I and 1J). Since clathrin mutants have fewer endocytic sites, concentrations of cytoplasmic endocytic proteins may be higher. The altered lifetimes of Las17p, Sla1p, and Abp1p patches in clathrin mutants could be due to increased concentrations of free patch proteins. However, a direct role for clathrin in regulating patch assembly and disassembly dynamics is also possible. Ede1p is a candidate to share clathrin's endocytic function, as its deletion phenotype is similar to that of clathrin mutants (Figures S1 and S2).

Evidence for Endocytic-Protein Modules

The endocytic proteins analyzed thus far can be divided into four groups based on their dynamic behaviors (Figures 3 and 7). We suggest that these groups represent dynamic protein modules, which cooperate to drive vesicle formation.

(1) The coat module consists of proteins that initially

assemble on the plasma membrane and then internalize ~200 nm with the forming vesicle before disassembling. This module contains clathrin, Sla1p, Pan1p, End3p, and Sla2p (Figure 7). The coat likely includes Ent1/2p and Yap1801/2p, but the dynamics of these proteins remain to be described (Newpher et al., 2005). The coat complex forms independently of actin, but its movement and disassembly requires actin polymerization (Figure 4).

(2) The actin module includes actin, Cap1/2p, Sac6p, Abp1p, and the Arp2/3 complex. The proteins in this module assemble into a conical, branched actin-filament meshwork (Rodal et al., 2005; Young et al., 2004). The actin meshwork and its associated vesicle are then released from the plasma membrane and start to move rapidly while actin filaments are being disassembled (Huckaba et al., 2004; Kaksonen et al., 2003). All of the proteins in this module depend on F-actin for localization (Figure 4).

(3) The WASP/Myo module consists of the yeast WASP homolog Las17p, the type I myosin Myo5p, and Bbc1p (Jonsdottir and Li, 2004). This module remains immotile at the plasma membrane at the site where actin is being polymerized and disassembles after the coat movement when actin polymerization has stopped. Assembly of Bbc1p and Las17p into this complex is independent of F-actin, but their disassembly depends on F-actin (Kaksonen et al., 2003).

(4) The amphiphysin module contains Rvs161p and Rvs167p. These proteins localize only briefly at endocytic sites, arriving after actin polymerization has started (Figures 3D and 6B). At first they are immotile, but they then move rapidly inward ~100 nm, after which they immediately dissipate. The 100 nm movement may correspond to vesicle scission. LatA experiments revealed that Rvs161-GFP is dependent upon F-actin for its localization. In contrast, Rvs167-GFP patches, uniquely, do not require actin for their turnover at the plasma membrane. They both do, however, require actin-driven invagination for their movement (Figures 4 and 6).

Functions of Endocytic Modules

Our analysis of endocytic-protein dynamics in deletion-mutant strains identified roles for 15 proteins in clathrin/actin-mediated endocytosis. The remaining endocytic proteins likely have functions that may not be detected by our screening method. Moreover, the functions of several endocytic proteins, including those that have paralogs (Table S1), may be redundant and likely mask defects in the single mutants. Further work is needed to uncover the roles of these proteins.

Coat-module proteins likely perform several functions, including cargo recruitment and actin-dynamics regulation. *SLA1* and *END3* deletions cause significant delays in actin-polymerization initiation, suggesting roles in regulating actin-polymerization initiation at endocytic sites (Figure 2B). This function could be mediated through Arp2/3 activators. Both Sla1p and End3p bind to the Arp2/3 activator Pan1p (Tang et al., 2000), and Sla1p also binds to the Arp2/3 activator, Las17p (Rodal et al., 2003). Sla1p also functions as an adaptor for receptor-mediated endocytic uptake (Howard et al., 2002). Perhaps actin polymerization is coordinated with cargo loading to maximize endocytic uptake efficiency.

Actin polymerization is needed for coat internalization (Kaksonen et al., 2003). We studied four actin module mutants, *sac6*Δ, *cap1*Δ, *cap2*Δ, and *abp1*Δ, and found evidence for several distinct functions. In the absence of the actin-filament-crosslinking protein, Sac6p, actin assembles with normal timing at endocytic sites, but the coat is not internalized. This suggests that filament crosslinking is required so that forces can be transmitted through the actin meshwork perpendicular to the cell surface. In *sac6*Δ cells, actin assembly still leads to disassembly of Sla1p, but not clathrin, suggesting that different disassembly mechanisms may exist for the proteins of the coat module.

Capping protein has been hypothesized to function in actin-polymerization-driven motility by limiting monomer addition to the most recently assembled, uncapped subset of barbed ends, thus increasing polymerization rates locally (Pantaloni et al., 2001). Consistent with this funneling model, the coat moves at a reduced rate in *cap1/2*Δ cells (Figure 2B). Capping protein might target actin monomer addition to new filaments close to the cell surface.

Despite demonstration that Abp1p activates the Arp2/3 complex in vitro (Goode et al., 2001), the *abp1*Δ phenotype suggests a role in endocytic-structure disassembly (Figure 2B). Consistent with this phenotype, Abp1p recruits Ark1p and Prk1p, protein kinases implicated in patch disassembly (Cope et al., 1999; Fazi et al., 2002; Sekiya-Kawasaki et al., 2003; Toshima et al., 2005), and the yeast synaptojanin, Sjl2, implicated in coat disassembly (Stefan et al., 2005), to endocytic sites. Furthermore, the *abp1*Δ phenotype is similar to, but less severe than, the phenotype of *ark1/prk1* mutants, which result in stabilization and aggregation of actin patches after internalization (Sekiya-Kawasaki et al., 2003).

Proteins of the WASP/Myo module can control actin-network growth by regulating actin-filament nucleation via the Arp2/3 complex. Las17p is required for endocytosis in yeast (Naqvi et al., 1998). Myo3/5p have also been implicated in Arp2/3 activation (Evangelista et al., 2000; Lechler et al., 2000), and cells lacking both myosins are defective in endocytosis and actin-patch movement (Geli and Riezman, 1996; Jonsdottir and Li, 2004; Smith et al., 2001). Bbc1p can inhibit Arp2/3 activation by Las17p in vitro (Rodal et al., 2003) and has been shown to bind to Myo3/5p (Mochida et al., 2002). In *bbc1*Δ cells, the actin-driven movement is enhanced, and a portion of Las17p moves together with the coat (Figure 5F). This suggests that Las17p interacts with the coat components and that Bbc1p may regulate this interaction.

The WASP/Myo module remains at the cell cortex and may first circumscribe the coat proteins and then decorate the rim of the coated pit as the coat proteins move inward off the cell surface. When the WASP/Myo module nucleates actin polymerization, these newly

formed actin filaments could then be tethered to the coat such that subsequent polymerization would push the coat, thus invaginating the underlying membrane. Sla2p and Pan1p are candidates for tethering the coat to actin filaments (McCann and Craig, 1997; Toshima et al., 2005).

The *SLA1* and *BBC1* deletion phenotypes described here support an in vivo role in regulating actin polymerization. However, the phenotypes are different, and these two proteins localize differently. Bbc1p joins Las17p at the endocytic site as Sla1p begins its actin-dependent inward movement away from Las17p. Therefore, Sla1p and Bbc1p might regulate the actin-nucleating machinery at different steps of the endocytic pathway. The combination of *bbc1*Δ and *sla1*Δ mutations leads to formation of dramatic actin protrusions that associate with, and dynamically project away from, the WASP/Myo module proteins at the cell surface (Figure 5). As these aberrant actin protrusions drive coated-vesicle internalization, we propose that they are exaggerations of the structures that drive normal endocytic internalization. Photobleaching showed that actin was polymerized at the plasma membrane (Figure 5E), and two-color imaging revealed that the coated vesicles moved off the cell surface at the same rate as actin-protrusion growth (Figure 5B and 5C). These observations suggest that actin polymerization at the plasma membrane generates the driving force for the coat movement, although the type I myosin motor may also contribute to this process. Surprisingly, the directionality of actin polymerization relative to the movement of the propelled object is opposite to that involved in *Listeria* or endosome motility (Taunton et al., 2000; Theriot et al., 1992). The actin structures present in *bbc1*Δ *sla1*Δ cells formed in two distinct phases (Figure 5). First, a bright immotile actin cloud formed at the plasma membrane. Next, continuing actin polymerization formed a dimmer actin protrusion that propelled the initial actin cloud inward. We speculate that these two phases may occur in wild-type cells, where they may be undetectable due to the resolution limits of light microscopy.

Amphiphysin-module proteins, Rvs161p and Rvs167p, contain BAR domains, which can bind and tubulate membranes in vitro (Peter et al., 2004). The Rvs proteins arrive after the actin marker Abp1p has started to accumulate but reach their peak fluorescence intensity together with Abp1p (Figures 6B and 6C), consistent with the timing of scission during mammalian endocytosis (Merrifield et al., 2005). This timing suggests that the short rapid movement of these proteins may coincide with scission. Supporting this possibility, in *bbc1*Δ *sla1*Δ mutant cells, Rvs167p localizes to the site of scission (Figure 6G). Moreover, both *rvs161*Δ and *rvs167*Δ cells frequently showed a retraction of the coat complex after the initial internalization movement. Given this phenotype and the localization of the Rvs proteins, we favor a model in which coat retraction is a result of a scission defect, wherein membrane tension retracts the coated invagination back to the cell surface when scission fails. Supporting this model, mammalian amphiphysin has been suggested to function with the scission factor dynamin (Takei et al., 1999). Further work is needed to rule out alternative explanations for the amphiphysin mutant phenotype. Additional factors must contribute to scission since only ~25% of endocytic sites are defective in amphiphysin mutants. Type I myosins and lipid regulation are other candidate scission factors (Jonsdottir and Li 2004; Stefan et al., 2005).

Experimental Procedures

Media and Strains

Yeast strains were grown in standard rich medium (YPD) or synthetic medium (SD) supplemented with appropriate amino acids. All strains were cultured at 25°C.

GFP or monomeric RFP (Campbell et al., 2002) tags were integrated chromosomally to generate C-terminal fusions of each protein as described in (Wach et al., 1997). All strains expressing fluorescent fusion proteins had growth properties similar to the corresponding untagged strains. Gene deletions were created by integrating a *Candida glabrata LEU2* or *URA3* selection casette to replace entire gene ORFs. Yeast strains are listed in Table S2. To generate endocytic deletion mutants for live-cell microscopy, we crossed strains from the MATα yeast deletion collection (ResGen) to strains DDY3056 and DDY3057. All crosses were sporulated, and two or three haploids both carrying a deletion and encoding a GFP-tagged protein were visually analyzed. To verify the phenotypes of *sla1*Δ, *end3*Δ, *bbc1*Δ, *rvs161*Δ, *rvs167*Δ, *sac6*Δ, *cap1*Δ, *cap2*Δ, and *abp1*Δ cells, we recreated these mutations by homologous recombination in the DDY1102 background expressing Sla1/Pan1-GFP and Abp1/Sac6-RFP.

FM4-64 and Lucifer Yellow Staining

FM4-64 staining was done in a flow chamber. The dye was solubilized in DMSO, diluted to 8 μM in synthetic medium, and perfused into a flow chamber to stain the plasma membrane of the cells. Imaging was performed immediately following the addition of the dye.

Lucifer yellow uptake assays were performed as described previously (Belmont and Drubin, 1998).

Live-Cell Imaging

For microscopy, cells were grown in SD without tryptophan (to minimize autofluorescence) at 25°C until early log phase. Cells were attached to concanavalin A-coated coverslips, which were sealed to slides with vacuum grease (Dow Corning). Imaging was done at room temperature using a Nikon TE300 or an Olympus IX81 microscope equipped with 100× NA1.4 objectives and Orca-100 or Orca II cameras (Hamamatsu). TIRF microscopy was done with an Olympus IX81 microscope equipped with a 100× NA1.65 lens and 488 nm argon-ion laser (Melles Griot). The excitation intensity was regulated by neutral density filters, and the images were acquired continuously at rates of 0.4–1 frames/s. Simultaneous two-color imaging was done using an image splitter (Optical Insight) to separate the red and green emission signals to two sides of the camera sensor using 565 nm dichroic mirror and 530/30 nm and 630/50 nm emission filters. To excite GFP, we used a 488 nm argon-ion laser; for RFP, we used a mercury lamp filtered through a 575/20 nm filter. The excitation beams from these two light sources were combined using a beam splitter. After each experiment, images of immobilized microbeads that fluoresce at both green and red wavelengths were captured. These images were used to align the cell images.

Photobleaching studies were done using a Zeiss 510 confocal microscope equipped with a 63× NA1.4 objective. A small region was bleached at full laser power followed by imaging at reduced excitation intensity.

Image Analysis

Image analysis was done as described previously (Kaksonen et al., 2003). Tracking of patches was done from single-color GFP movies to achieve the best signal-to-noise ratio. ImageJ (http://rsb.info.nih.gov/ij/) was used for preparing kymographs and for general manipulation of images and movies.

Supplemental Data

Supplemental Data include two tables, three figures, and eight movies and can be found with this article online at http://www.cell.com/cgi/content/full/123/2/305/DC1/.

Acknowledgments

The authors wish to thank Claire Zhang, Yidi Sun, Linda Lee, Isabelle Le Blanc, Voytek Okreglak, Brian Young, Adam Martin, Stefan Westermann, and Georjana Barnes for critical comments on the manuscript; Roger Tsien for the mRFP plasmid; and Rick Staples from Olympus for microscopy support. This work was supported by NIH grants R01GM50399 and R01GM42759 and NIH Shared Instrumentation Grant S10-RR019290 to D.G.D. and by a Sigrid Jusélius Foundation and Finnish Academy fellowship to M.K.

Received: April 12, 2005
Revised: August 8, 2005
Accepted: September 20, 2005
Published: October 20, 2005

References

Adams, A.E., Botstein, D., and Drubin, D.G. (1991). Requirement of yeast fimbrin for actin organization and morphogenesis in vivo. Nature *354*, 404–408.

Amatruda, J.F., Gattermeir, D.J., Karpova, T.S., and Cooper, J.A. (1992). Effects of null mutations and overexpression of capping protein on morphogenesis, actin distribution and polarized secretion in yeast. J. Cell Biol. *119*, 1151–1162.

Ayscough, K.R., Stryker, J., Pokala, N., Sanders, M., Crews, P., and Drubin, D.G. (1997). High rates of actin filament turnover in budding yeast and roles for actin in establishment and maintenance of cell polarity revealed using the actin inhibitor latrunculin-A. J. Cell Biol. *137*, 399–416.

Baggett, J.J., and Wendland, B. (2001). Clathrin function in yeast endocytosis. Traffic *2*, 297–302.

Balguerie, A., Sivadon, P., Bonneu, M., and Aigle, M. (1999). Rvs167p, the budding yeast homolog of amphiphysin, colocalizes with actin patches. J. Cell Sci. *112*, 2529–2537.

Belmont, L.D., and Drubin, D.G. (1998). The yeast V159N actin mutant reveals roles for actin dynamics in vivo. J. Cell Biol. *142*, 1289–1299.

Campbell, R.E., Tour, O., Palmer, A.E., Steinbach, P.A., Baird, G.S., Zacharias, D.A., and Tsien, R.Y. (2002). A monomeric red fluorescent protein. Proc. Natl. Acad. Sci. USA *99*, 7877–7882.

Chu, D.S., Pishvaee, B., and Payne, G.S. (1996). The light chain subunit is required for clathrin function in Saccharomyces cerevisiae. J. Biol. Chem. *271*, 33123–33130.

Cope, M.J., Yang, S., Shang, C., and Drubin, D.G. (1999). Novel protein kinases Ark1p and Prk1p associate with and regulate the cortical actin cytoskeleton in budding yeast. J. Cell Biol. *144*, 1203–1218.

Doyle, T., and Botstein, D. (1996). Movement of yeast cortical actin cytoskeleton visualized in vivo. Proc. Natl. Acad. Sci. USA *93*, 3886–3891.

Ehrlich, M., Boll, W., Van Oijen, A., Hariharan, R., Chandran, K., Nibert, M.L., and Kirchhausen, T. (2004). Endocytosis by random initiation and stabilization of clathrin-coated pits. Cell *118*, 591–605.

Engqvist-Goldstein, A.E., and Drubin, D.G. (2003). Actin assembly and endocytosis: from yeast to mammals. Annu. Rev. Cell Dev. Biol. *19*, 287–332.

Evangelista, M., Klebl, B.M., Tong, A.H., Webb, B.A., Leeuw, T., Leberer, E., Whiteway, M., Thomas, D.Y., and Boone, C. (2000). A role for myosin-I in actin assembly through interactions with Vrp1p, Bee1p, and the Arp2/3 complex. J. Cell Biol. *148*, 353–362.

Fazi, B., Cope, M.J., Douangamath, A., Ferracuti, S., Schirwitz, K., Zucconi, A., Drubin, D.G., Wilmanns, M., Cesareni, G., and Castagnoli, L. (2002). Unusual binding properties of the SH3 domain of the yeast actin-binding protein Abp1: structural and functional analysis. J. Biol. Chem. *277*, 5290–5298.

Geli, M.I., and Riezman, H. (1996). Role of type I myosins in receptor-mediated endocytosis in yeast. Science *272*, 533–535.

Goode, B.L., Rodal, A.A., Barnes, G., and Drubin, D.G. (2001). Activation of the Arp2/3 complex by the actin filament binding protein Abp1p. J. Cell Biol. *153*, 627–634.

Holtzman, D.A., Yang, S., and Drubin, D.G. (1993). Synthetic-lethal interactions identify two novel genes, SLA1 and SLA2, that control membrane cytoskeleton assembly in Saccharomyces cerevisiae. J. Cell Biol. *122*, 635–644.

Howard, J.P., Hutton, J.L., Olson, J.M., and Payne, G.S. (2002). Sla1p serves as the targeting signal recognition factor for NPFX(1,2)D-mediated endocytosis. J. Cell Biol. *157*, 315–326.

Huckaba, T.M., Gay, A.C., Pantalena, L.F., Yang, H.C., and Pon, L.A. (2004). Live cell imaging of the assembly, disassembly, and actin cable-dependent movement of endosomes and actin patches in the budding yeast, Saccharomyces cerevisiae. J. Cell Biol. *167*, 519–530.

Jonsdottir, G.A., and Li, R. (2004). Dynamics of yeast Myosin I: evidence for a possible role in scission of endocytic vesicles. Curr. Biol. *14*, 1604–1609.

Kaksonen, M., Sun, Y., and Drubin, D.G. (2003). A pathway for association of receptors, adaptors, and actin during endocytic internalization. Cell *115*, 475–487.

Kim, K., Yamashita, A., Wear, M.A., Maeda, Y., and Cooper, J.A. (2004). Capping protein binding to actin in yeast: biochemical mechanism and physiological relevance. J. Cell Biol. *164*, 567–580.

Lechler, T., Shevchenko, A., and Li, R. (2000). Direct involvement of yeast type I myosins in Cdc42-dependent actin polymerization. J. Cell Biol. *148*, 363–373.

Martin, A.C., Xu, X.P., Rouiller, I., Kaksonen, M., Sun, Y., Belmont, L., Volkmann, N., Hanein, D., Welch, M., and Drubin, D.G. (2005). Effects of Arp2 and Arp3 nucleotide-binding pocket mutations on Arp2/3 complex function. J. Cell Biol. *168*, 315–328.

McCann, R.O., and Craig, S.W. (1997). The I/LWEQ module: a conserved sequence that signifies F-actin binding in functionally diverse proteins from yeast to mammals. Proc. Natl. Acad. Sci. USA *94*, 5679–5684.

Merrifield, C.J., Feldman, M.E., Wan, L., and Almers, W. (2002). Imaging actin and dynamin recruitment during invagination of single clathrin-coated pits. Nat. Cell Biol. *4*, 691–698.

Merrifield, C.J., Qualmann, B., Kessels, M.M., and Almers, W. (2004). Neural Wiskott Aldrich Syndrome Protein (N-WASP) and the Arp2/3 complex are recruited to sites of clathrin-mediated endocytosis in cultured fibroblasts. Eur. J. Cell Biol. *83*, 13–18.

Merrifield, C.J., Perrais, D., and Zenisek, D. (2005). Coupling between clathrin-coated-pit invagination, cortactin recruitment, and membrane scission observed in live cells. Cell *121*, 593–606.

Mochida, J., Yamamoto, T., Fujimura-Kamada, K., and Tanaka, K. (2002). The novel adaptor protein, Mti1p, and Vrp1p, a homolog of Wiskott-Aldrich syndrome protein-interacting protein (WIP), may antagonistically regulate type I myosins in Saccharomyces cerevisiae. Genetics *160*, 923–934.

Naqvi, S.N., Zahn, R., Mitchell, D.A., Stevenson, B.J., and Munn, A.L. (1998). The WASp homologue Las17p functions with the WIP homologue End5p/verprolin and is essential for endocytosis in yeast. Curr. Biol. *8*, 959–962.

Newpher, T.M., Smith, R.P., Lemmon, V., and Lemmon, S.K. (2005). In vivo dynamics of clathrin and its adaptor-dependent recruitment to the actin-based endocytic machinery in yeast. Dev. Cell *9*, 87–98.

Pantaloni, D., Le Clainche, C., and Carlier, M.F. (2001). Mechanism of actin-based motility. Science *292*, 1502–1506.

Payne, G.S., Baker, D., van Tuinen, E., and Schekman, R. (1988). Protein transport to the vacuole and receptor-mediated endocytosis by clathrin heavy chain-deficient yeast. J. Cell Biol. *106*, 1453–1461.

Peter, B.J., Kent, H.M., Mills, I.G., Vallis, Y., Butler, P.J., Evans, P.R.,

and McMahon, H.T. (2004). BAR domains as sensors of membrane curvature: the amphiphysin BAR structure. Science *303*, 495–499.

Rodal, A.A., Manning, A.L., Goode, B.L., and Drubin, D.G. (2003). Negative regulation of yeast WASp by two SH3 domain-containing proteins. Curr. Biol. *13*, 1000–1008.

Rodal, A.A., Kozubowski, L., Goode, B.L., Drubin, D.G., and Hartwig, J.H. (2005). Actin and septin ultrastructures at the budding yeast cell cortex. Mol. Biol. Cell *16*, 372–384.

Sekiya-Kawasaki, M., Groen, A.C., Cope, M.J., Kaksonen, M., Watson, H.A., Zhang, C., Shokat, K.M., Wendland, B., McDonald, K.L., McCaffery, J.M., and Drubin, D.G. (2003). Dynamic phosphoregulation of the cortical actin cytoskeleton and endocytic machinery revealed by real-time chemical genetic analysis. J. Cell Biol. *162*, 765–772.

Sivadon, P., Bauer, F., Aigle, M., and Crouzet, M. (1995). Actin cytoskeleton and budding pattern are altered in the yeast rvs161 mutant: the Rvs161 protein shares common domains with the brain protein amphiphysin. Mol. Gen. Genet. *246*, 485–495.

Smith, M.G., Swamy, S.R., and Pon, L.A. (2001). The life cycle of actin patches in mating yeast. J. Cell Sci. *114*, 1505–1513.

Stefan, C.J., Padilla, S.M., Audhya, A., and Emr, S.D. (2005). The phosphoinositide phosphatase Sjl2 is recruited to cortical actin patches in the control of vesicle formation and fission during endocytosis. Mol. Cell. Biol. *25*, 2910–2923.

Takei, K., Slepnev, V.I., Haucke, V., and De Camilli, P. (1999). Functional partnership between amphiphysin and dynamin in clathrin-mediated endocytosis. Nat. Cell Biol. *1*, 33–39.

Tang, H.Y., Munn, A., and Cai, M. (1997). EH domain proteins Pan1p and End3p are components of a complex that plays a dual role in organization of the cortical actin cytoskeleton and endocytosis in Saccharomyces cerevisiae. Mol. Cell. Biol. *17*, 4294–4304.

Tang, H.Y., Xu, J., and Cai, M. (2000). Pan1p, End3p, and S1a1p, three yeast proteins required for normal cortical actin cytoskeleton organization, associate with each other and play essential roles in cell wall morphogenesis. Mol. Cell. Biol. *20*, 12–25.

Taunton, J., Rowning, B.A., Coughlin, M.L., Wu, M., Moon, R.T., Mitchison, T.J., and Larabell, C.A. (2000). Actin-dependent propulsion of endosomes and lysosomes by recruitment of N-WASP. J. Cell Biol. *148*, 519–530.

Theriot, J.A., Mitchison, T.J., Tilney, L.G., and Portnoy, D.A. (1992). The rate of actin-based motility of intracellular Listeria monocytogenes equals the rate of actin polymerization. Nature *357*, 257–260.

Toshima, J., Toshima, J.Y., Martin, A.C., and Drubin, D.G. (2005). Phosphoregulation of Arp2/3-dependent actin assembly during receptor-mediated endocytosis. Nat. Cell Biol. *7*, 246–254.

Wach, A., Brachat, A., Alberti-Segui, C., Rebischung, C., and Philippsen, P. (1997). Heterologous HIS3 marker and GFP reporter modules for PCR-targeting in Saccharomyces cerevisiae. Yeast *13*, 1065–1075.

Warren, D.T., Andrews, P.D., Gourlay, C.W., and Ayscough, K.R. (2002). Sla1p couples the yeast endocytic machinery to proteins regulating actin dynamics. J. Cell Sci. *115*, 1703–1715.

Yarar, D., Waterman-Storer, C.M., and Schmid, S.L. (2005). A dynamic actin cytoskeleton functions at multiple stages of clathrin-mediated endocytosis. Mol. Biol. Cell *16*, 964–975.

Young, M.E., Cooper, J.A., and Bridgman, P.C. (2004). Yeast actin patches are networks of branched actin filaments. J. Cell Biol. *166*, 629–635.